Growth and Helicity of Noncentrosymmetric Cu_2OSeO_3 Crystals

Aisha Aqeel, Jan Sahliger, Guowei Li, Jacob Baas, Graeme R. Blake, Thomas T. M. Palstra, and Christian H. Back*

Cu_2OSeO_3 single crystals are grown with an optimized chemical vapor transport technique using $SeCl_4$ as a transport agent (TA). The optimized growth method allows to selectively produce large high-quality single crystals. The method is shown to consistently produce Cu_2OSeO_3 crystals of maximum size $8 \times 7 \times 4$ mm with a transport duration of around three weeks. It is found that this method, with $SeCl_4$ as TA, is more efficient and simple compared with the commonly used growth techniques reported in literature with HCl gas as TA. The Cu_2OSeO_3 crystals have very high quality and their absolute structures are fully determined by simple single-crystal X-ray diffraction. Enantiomeric crystals with either left- or right-handed chiralities are observed. The magnetization and ferromagnetic resonance data show the same magnetic phase diagram as reported earlier.

1. Introduction

Investigation of complex magnetic systems[1] is generally limited by an inability to obtain sufficiently large, pure high-quality crystals. This is especially true for the noncentrosymmetric magnets with chirality. In this class of materials, the interactions that may lead to symmetry breaking magnetic order do not cancel each other when evaluated over the unit cell. The most well-studied chiral systems are $MnSi$[2,3] $Mn_{1-x}Fe_xGe$,[4] $FeGe$,[5] and semiconducting $Fe_{1-x}Co_xSi$.[6] In these chiral magnets, the principal magnetic phases are helical phases, a single-domain conical phase, and a skyrmion state (known as A-phase). They appear in a small magnetic field–temperature (B–T) pocket close to transition temperature T_c. In the chiral atomic framework of this crystal family, the orbital motions of localized electrons also take helical paths. The neighboring spins of localized electrons are coupled by the relativistic spin–orbit interaction called Dzyaloshinskii–Moriya (DM) interaction.[7,8] As the sign of the DM interaction is determined by the chemical composition, it emphasizes that the magnetic chirality is intrinsically dependent on the lattice handedness. It has been shown experimentally in $Mn_{1-x}Fe_xGe$ crystals that skyrmion helicity is directly determined by the crystal helicity.[4]

Cu_2OSeO_3 is one of the most important members of the chiral group with the $P2_13$ chiral cubic crystal structure. It is the first insulator in which the skyrmion lattice has been observed[9,10] with a very similar B–T phase diagram as the other related members of this chiral group. Recently, some new magnetic phases like tilted conical spiral,[11] low-temperature skyrmion lattice phase,[12] and elongated skyrmions[13] have been observed in Cu_2OSeO_3. The insulating behavior of this magnetic material makes the study of the decisive role of crystal helicity especially more interesting by excluding other contributions due to conduction electrons. To understand the unique magnetic structure of Cu_2OSeO_3, several different techniques have been used including muon spin rotation/relaxation (μSR),[14] Lorentz transmission electron microscope,[10] ac-susceptibility measurements,[15] terahertz electron spin resonance,[16] and time-resolved magneto-optics.[17] Recently, generation of spin currents has been studied in Cu_2OSeO_3 by spin-pumping experiments.[18]

Considering the large interest in the magnetic properties of Cu_2OSeO_3, it is important to look for new, efficient, and fast single-crystal growth techniques. Conventionally, Cu_2OSeO_3 crystals are grown by the vapor transport method with HCl gas as transport agent (TA). With this growth method only one helicity has been reported.[19] The other helicity has not been reported to the best of our knowledge. It is known that the structural and magnetic chiralities for Cu_2OSeO_3 crystals are directly

A. Aqeel, J. Sahliger, C. H. Back
Department of Physics
Technical University of Munich
Garching 85748, Germany
E-mail: christian.back@tum.de

G. Li
Max Planck Institute for Chemical Physics of Solids
Dresden 01187, Germany

J. Baas, G. R. Blake, T. T. M. Palstra[+]
Zernike Institute for Advanced Materials
University of Groningen
Nijenborgh 4, Groningen 9747 AG, The Netherlands

C. H. Back
Munich Center for Quantum Science and Technology (MCQST)
München 80799, Germany

[ID] The ORCID identification number(s) for the author(s) of this article can be found under https://doi.org/10.1002/pssb.202100152.

[+]Present address: Faculty of Science and Technology (TNW), University of Twente, Enschede 7522NB, The Netherlands

related with each other.[19] Therefore to use both magnetic chiralities, it is needed to improve the growth techniques not only to speed up the growth rate but also to get crystals with both chiralities. Here, we report a new and fast way for the growth of Cu_2OSeO_3 single crystals with $SeCl_4$ as TA. We observed very-high-quality crystal growth yielding both chiralities with this new growth technique. The crystal structure of Cu_2OSeO_3 crystals has been studied before[20–22] with different diffraction techniques. Here, we used the simplest single-crystal X-ray diffraction (XRD) to establish the absolute structures for both handedness, which also emphasizes good quality of the crystals.

2. Experimental Section

Single crystals of Cu_2OSeO_3 were grown by the standard chemical vapor transport method. However, the novelty of this growth was the use of selenium tetrachloride ($SeCl_4$) as a TA. Previously, $SeCl_4$ was mainly used to grow molybdenum and tungsten diselenides. In literature, Cu_2OSeO_3 is usually grown by HCl gas.[23] Here, we report the growth of chiral magnets with $SeCl_4$ as TA, which is new and different from literature.[24] For growth, transparent quartz ampoules (30 mm inside diameter, 30 cm length) were used. They were first carefully cleaned with ethanol, acetone, 10% HF, and demiwater and dried overnight at 200 °C before the charge was introduced. $SeCl_4$ is very hygroscopic; therefore, it was weighed and introduced into the transport tubes in a glove box in nitrogen atmosphere. Mixtures of high-purity CuO (Alfa-Aldrich, 99.995%) and SeO_2 (Alfa-Aldrich, 99.999%) powders in a molar ratio of 2:1 were sealed in an evacuated quartz ampoule with $0.54 \times g$ of $SeCl_4$ (Alfa-Aldrich, 99.5%). After a few minutes of degassing, the part of the ampoule containing chemicals was immersed in liquid nitrogen and subsequently evacuated and sealed after the chemicals cooled below evaporation temperatures. The ampoule was then placed horizontally into a tubular three-zone furnace having 18 cm-long zones separated by a distance of 3 cm. The temperature of the furnace was raised gradually by 50 °C h^{-1} to 600 °C. To get rid of unwanted nucleation centers, a reverse temperature gradient was applied by adjusting the temperature of the source zone (T_{hot}) to 610 °C and the deposition zone (T_{cold}) to 660 °C for 24 h. Afterward, T_{hot} and T_{cold} were adjusted to 610 °C and 570 °C, respectively, for growth. These furnaces were regulated by a PID electronic regulator (SHINKO) with ±0.5 °C temperature stability at 500–650 °C. After 2 weeks, shiny crystals were seen at the deposition zone. After 4 weeks, the ampoules were quenched at the source zone so that all gas vapors condensed at the source zone. The extreme hygroscopic nature of $SeCl_4$ resulted in the presence of water in the ampoules, in spite of all precautions taken. The presence of water created the vapor phase of hydrogen chloride (HCl) and chalcogen oxichloride (SeOCl), thus making the analysis of the transport mechanism more complex. However, we observed that the presence of moisture slowed down the transport process. This transport method with $SeCl_4$ resulted in reasonably big and thick crystals. To compare the efficiency of the growth method, we also synthesized the crystals with HCl gas as TA, as reported in literature.[23] The growth conditions are shown in **Table 1**. The crystal structure of Cu_2OSeO_3 crystals was investigated by single-crystal XRD

Table 1. Growth conditions for Cu_2OSeO_3 with chemical vapor transport growth method for different TAs.

TA	T_{hot} [°C]	T_{cold} [°C]	Duration of growth [d]	Maximum size of crystals [mm³]
HCl[23]	620	580	49	130–150
$SeCl_4$	610	570	23	210–224

on a D8 Venture diffractometer. The crystal quality was checked by collection of a full sphere of XRD data using high-precision scans. The morphology and elemental analysis were examined using Philips XL 30 scanning electron microscopy (SEM), equipped with an energy-dispersive spectrometer (EDS) system, which was operated at an accelerating voltage of 20 kV. The magnetization measurements were carried out using a Quantum Design magnetic measurement system (MPMS-XL) 7 SQUID magnetometer.

To further study the phase magnetic phase diagram of Cu_2OSeO_3, we carried out ferromagnetic resonance (FMR) measurements using a broadband spin-wave spectroscopy technique[13,25] on both HCl and $SeCl_4$ grown crystals. For this purpose, we used two polished crystals with similar dimensions: HCl-grown sample with size $1.5 \times 2.5 \times 0.5$ mm³ and $SeCl_4$-grown crystals with size $2.9 \times 2.7 \times 1$ mm³. The crystals were polished using the technique reported in the study by Aqeel et al.[26] The coplanar waveguides (CPWs) with a signal line of 50 μm width and gap of 25 μm width were patterned. The CPWs were directly patterned onto the oriented polished crystals with (110) and (111) surfaces, respectively. They were patterned by e-beam lithography followed by e-beam evaporation of Ti (10 nm)/Au (150 nm). The excitation field distribution of the CPWs is shown in Figure 4b. The samples with CPWs were mounted on a continuous-flow cryostat. A vector network analyzer (VNA) was used to measure the resonance signals. The temperature reading of the cryostat was different from the MPMS system used to measure the magnetization data due to the placement of the temperature sensor. The temperature difference (7–10 K) between both setups was adjusted in the experiment. A rotatable electromagnet was used to provide the static magnetic field up to 500 mT.

3. Results

A tiny single crystal grown with $SeCl_4$ was selected for morphology and element analysis, as shown in **Figure 1**a. The as-synthesized crystal has a rough surface with many tiny nanoparticles attached on it. The molar ratios of Se, Cu, and O are determined to be very close to the stoichiometric Cu_2OSeO_3 sample. Furthermore, the EDS elemental mapping (Figure 1b–d) demonstrates that the Cu, O, and Se atoms are uniformly distributed, which unambiguously reveals the uniformity of the single crystal. That is, a homogeneous and high-quality sample was successfully synthesized with such a simple method. **Table 2** shows the parameters used to establish the absolute structure of Cu_2OSeO_3 single crystals. Cu_2OSeO_3 crystals display the $P2_13$ space group and the ions occupy the Wyckoff positions (WFs)
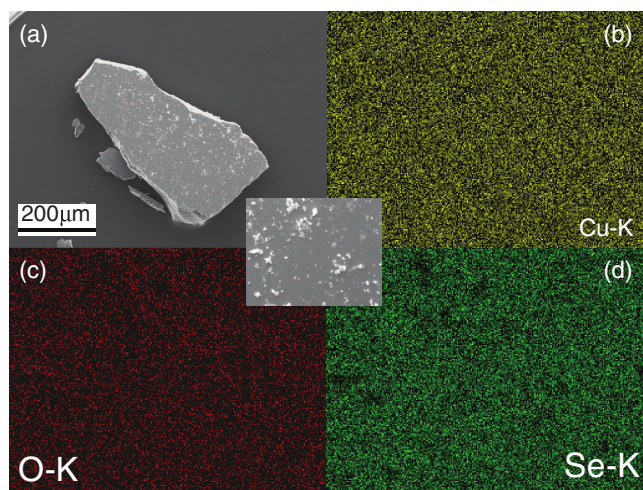
Figure 1. a) The SEM image of a typical single crystal. EDS elemental mapping for b) Cu, c) O, and d) Se elements in the as-synthesized crystal. The inset shows the scanning area for element mapping.

Table 2. Crystallographic data and structure refinement for Cu_2OSeO_3 single crystals.

Temperature	100 K
Crystal system	Cubic
Space group	$P2_13$
Wave length	0.7107 Å
Unit cell dimension a	8.9446 Å
θ range for data collection	3.147°–32.25°
Limiting indices	$-13 \leq h \leq 13$
	$-11 \leq k \leq 11$
	$-13 \leq l \leq 13$
Reflections collected/unique	0.0367
Final R indices [$I > 2\sigma(I)$]	0.0312
Absolute structure parameter	$-0.01(2)$

that are shown in **Table 3**. The precision scans of XRD for full-sphere approximation show the high quality of Cu_2OSeO_3 single crystals without any twinning.

The chirality of the crystals has been characterized by the Flack parameter analysis. The Flack parameter is defined for a racemic twin of noncentrosymmetric crystals as the ratio between the scattering power of the two opposite-handed domains, giving rise to a resonant contribution in the X-ray-scattering amplitudes. A Flack parameter equal to zero corresponds to a single domain of the chiral structure (enantiopure) and a Flack parameter equal to 1 represents a single domain structure but with opposite chiralities. The Flack parameter x is determined simultaneously with the atomic coordinates and atomic displacement parameters during the least-squares refinement of the crystal structure, using the twin model and thus enabling to determine the absolute structure of the crystal of a pure enantiomeric sample. The Flack parameter x for intensities of hkl reflections is as follows.

$$I_{hkl}^{calc} = (1 - x)|F_{hkl}|^2 + x|F_{-h-k-l}|^2 \tag{1}$$

Here, $|F_{hkl}|$ and $|F_{-h-k-l}|$ represent the structure factors. The full sphere of Bragg reflections was used for refinement. Results of least-square refinement gives a Flack x of 0.013(17), indicating two absolute structures having opposite chirality. The deviation factor is defined as

$$R_1 = \Sigma(|F_{obs}| - |F_{calc}|)/\Sigma|F_{obs}| \tag{2}$$

The reliability factors R_1 and wR_2, between the model and the data set, were found to be 0.0217 and 0.1473, respectively. We measured eight crystals to resolve the absolute structure, in which we found five right-handed and three left-handed enantiomers. The atomic coordinates for absolute structures for left-handed and right-handed enantiomers of Cu_2OSeO_3 (**Figure 2**) are shown in Table 3.

Figure 3a shows the temperature dependence of field-cooled magnetization measurements under an applied field H varying from 100 to 1500 Oe with a $T_c \approx 60\,K$.

The FMR spectra were measured as reported earlier[13] and the background-free transmission signal was defined as $|\Delta S_{21}|^2 = (|S_{21}(H) - |S_{21}(H_0)|)^2$. $S_{21}(H)$ and $S_{21}(H_0)$ are the complex transmissions measured with a VNA at fixed magnetic fields H and H_0, respectively. An example of such spectra measured for HCl- and $SeCl_4$-grown samples is shown in **Figure 4**d,e, respectively. These spectra are used to construct the high-temperature magnetic phase diagram of Cu_2OSeO_3 shown in Figure 4f.

Table 3. Atomic coordinates and WFs for Cu_2OSeO_3 for both handedness.

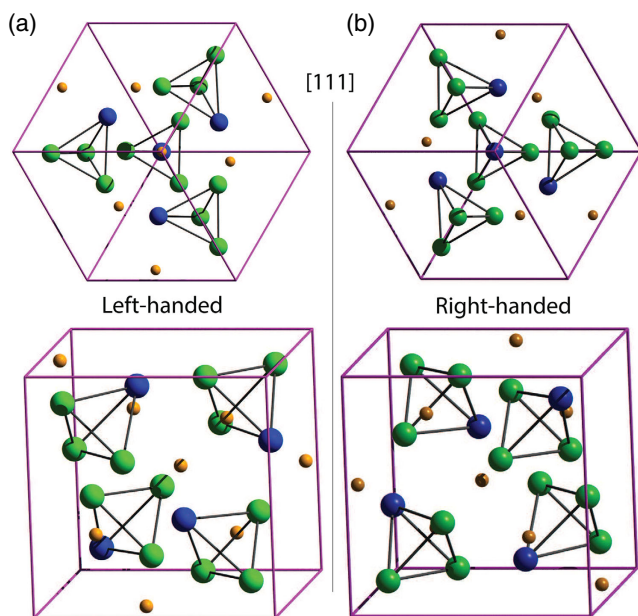|	WP	Right handed			Left handed		
		x	y	z	x	y	z
Cu (1)	4a	0.88589(3)	0.88589(3)	0.88589(3)	0.11404(4)	0.11404(4)	0.11404(4)
Cu (2)	12b	0.13439(3)	0.12108(3)	0.87247(3)	0.86549(4)	0.87895(4)	0.12754(4)
Se (1)	4a	0.45963(3)	0.45963(3)	0.45963(3)	0.54031(4)	0.54031(4)	0.54031(4)
Se (2)	4a	0.21201(3)	0.21201(3)	0.21201(3)	0.78802(4)	0.78802(4)	0.78802(4)
O (1)	4a	0.01031(3)	0.01031(3)	0.01031(3)	0.98974(3)	0.98974(4)	0.98974(3)
O (2)	12b	0.76232(2)	0.76232(2)	0.76232(2)	0.23730(3)	0.23730(4)	0.23730(3)
O (3)	4a	0.27029(2)	0.48318(2)	0.46954(2)	0.72971(3)	0.51663(4)	0.53014(3)
O (4)	12b	0.27257(2)	0.18681(2)	0.03276(2)	0.72786(3)	0.81329(4)	0.96738(3)

Figure 2. The two chiral crystal structures of Cu_2OSeO_3 where green and blue spheres represent Cu(1) and Cu(2) atoms. The top views are along the body diagonal of the cube (along [111] axis). a) Right-handed and b) left-handed crystals.

4. Discussion

The vapor transport technique[23] commonly used for the growth of Cu_2OSeO_3 single crystals is relatively slow and complex due to use of the HCl gas as TA. However, the method reported in this article is very simple and easy due to use of solid TA $SeCl_4$ and is also found to be relatively fast. A disadvantage of $SeCl_4$ TA could be the strong silica attack and its strong hygroscopic nature, which can be easily settled using the TA in an inert and dry atmosphere. $SeCl_4$ is frequently used in the past as an efficient TA for the growth of diselenides WSe_2 and $MoSe_2$.[24,27,28] Like $SeCl_4$, $TeCl_4$ can also be an efficient TA. $TeCl_4$ is more stable and less hygroscopic compared with $SeCl_4$ which makes it a more suitable TA compared with $SeCl_4$ for vapor transport growth. However, $TeCl_4$ can dope the crystals and therefore, $SeCl_4$ is more suitable for growth of undoped Cu_2OSeO_3 crystals. The decomposition of $SeCl_4$ will give a mixture of selenium and dichlorine that can result in possible gaseous oxygen compounds during transport of $SeCl_4$, which can be SeO_2, $SeOCl_2$, and SeO. Chlorine resulting from the decomposition of $SeCl_4$ probably plays an efficient role in transport but the role of the selenium is not very clear in transport. In the case of the presence of water, the transport would be more complicated by also involving HCl vapors. We observed a clear decrease in the deposition rate by exposing the $SeCl_4$ TA to the air.

The absolute structures were solved for six different crystals, grown with $SeCl_4$ as TA. During refinement, the Goodness of Fit (GooF) was found to be 0.9–1.03 and the scale factor K is 0.95–1.0, which confirms the high quality of these crystals. Four out of six analyzed crystals showed the same helicity and the other two crystals showed the opposite. The helicity can be defined from the WF of magnetic ions. In the case of Cu_2OSeO_3, Cu(1) and Cu(2) ions are located at $4a$ and $12b$ WF, as shown in Table 3. The $4a$ WF of Cu(1) in Cu_2OSeO_3 is $(x, x, x/0.5 + x, 0.5-x, -x/-x, 0.5 + x, 0.5-x/0.5-x, -x, 0.5 + x)$, where $x \approx 0.136$ or $x \approx 1-0.136 = 0.863$, corresponding to two enantiomers. The crystals having Cu(1) at $x = 0.863$ are
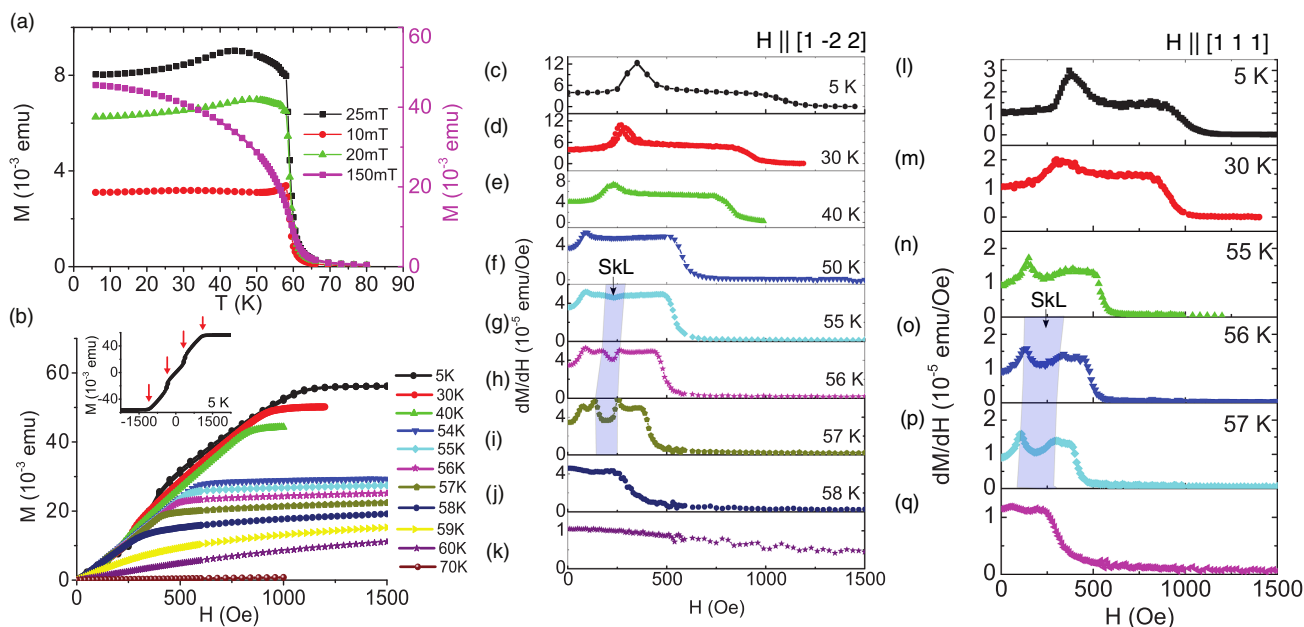

Figure 3. a) Temperature dependences of the field-cooled magnetic susceptibilities in different applied magnetic fields along [001] direction. b) Magnetic field dependence of the magnetization at different temperatures, with magnetic field applied along [1–22] direction. The inset shows the slope-change behavior at the fields ≈ 350 and 1100 Oe at 5 K, as indicated by arrows. The dM/dH versus H at different temperatures with magnetic field applied along c–k) [1–22] and l–q) [111] crystallographic directions. The shaded region represents the skyrmion lattice phase.
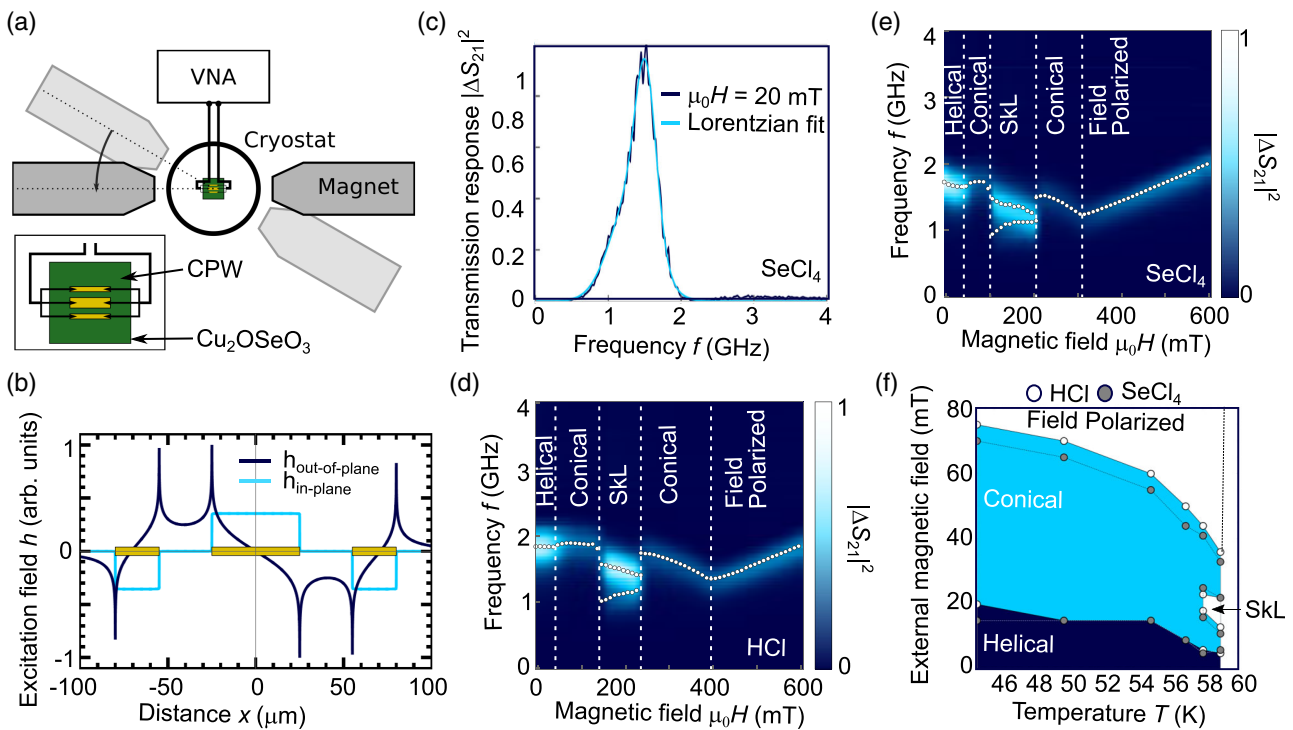
Figure 4. Schematics of the broadband FMR setup with a VNA, low-temperature measurement setup (cryostat), and a rotatable electromagnet. The inset shows the schematics of the CPW structured directly onto the sample surface. The static magnetic field H is applied along the CPW within the plane of the sample along the [1–11] crystallographic direction of Cu_2OSeO_3. b) Field distribution of the CPW. c) Transmission difference $\Delta|S_{21}|^2$ as a function of frequency measured at 20 mT at 5 K. d,e) Color-coded resonance map obtained from the line scans of the transmission response measured as a function of frequency at 58 K for the HCl- and $SeCl_4$-grown samples. f) The magnetic phase diagram of Cu_2OSeO_3 single crystals obtained by applying static magnetic field along [1–11] crystallographic direction of Cu_2OSeO_3. The phase boundaries (dots) are extracted from the resonance spectra shown in (d,e).

defined as right-handed enantiomer and others with $x = 0.136$ as left-handed enantiomer, as shown in Table 3. The structure of Cu_2OSeO_3 with the same set of coordinates for the right-handed crystals shown in Table 3 is also defined as right-handed in the study by Dyadkin et al.[19] There, the crystals are defined as right handed on the basis of similarity of $4a$ WF of Cu(1) ion in Cu_2OSeO_3 and Mn in MnSi (right handed).

The crystal helicity can also be defined by considering the closeness of the structural symmetry of the $P2_13$ space group with the absolute structure of $P4_132$, as proposed in the study by Chizhikov et al.[29] $P4_132$ space group contains only right-handed screw axes 4_1; therefore, the right-handed crystals of $P2_13$ space group can be easily distinguished by comparison. The same approach is also mentioned for B20 structures.[30] The set of coordinates determined with this definition for right-handed crystals is found to be consistent with the obtained absolute structure for the right-handed crystals, as shown in Table 3.

The magnetization and resonance data shown in Figure 3, 4 show the presence of the skyrmion lattice phase along with other magnetic phases of Cu_2OSeO_3. To determine the linewidths and peak positions from the transmission signal, Lorentzian peak fitting was used. An example of such peak fitting is shown in Figure 4c. The resonance spectra measured for both samples grown with HCl and $SeCl_4$ qualitatively show no clear difference (see Figure 4d,e). For both samples, resonance signal with

similar linewidth is observed, confirming that the crystals grown with the new method have the same damping as those grown with HCl.[31] The phase boundaries of the skyrmion lattice for both samples grown with HCl and $SeCl_4$ coincide with each other (see Figure 4f).

5. Conclusion

We have demonstrated a simple route that allows the growth of Cu_2OSeO_3 single crystals in a relatively short duration. The XRD analysis shows high quality of single crystals. We observed both right-handed and left-handed enantiomers of Cu_2OSeO_3 and the absolute structure was fully determined by the Flack parameter analysis of the refined XRD pattern. The growth of crystals with both left- and right-handed structural chiralities can be useful to understanding the coupling between structural and magnetic chiralities. The understanding of coupling is important to control the magnetic textures such as skyrmions for spintronics applications.

Conflict of Interest

Data Availability Statement

Keywords

[1] F. Qian, H. Wilhelm, A. Aqeel, T. T. M. Palstra, A. J. E. Lefering, E. H. Brück, C. Pappas, *Phys. Rev. B* **2016**, *94* 064418.

[2] S. Mühlbauer, B. Binz, F. Jonietz, C. Pfleiderer, A. Rosch, A. Neubauer, R. Georgii, P. Böni, *Science* **2009**, *323*, 915.

[3] F. Jonietz, S. Mühlbauer, C. Pfleiderer, A. Neubauer, W. Münzer, A. Bauer, T. Adams, R. Georgii, P. Böni, R. A. Duine, K. Everschor, M. Garst, A. Rosch, *Science* **2010**, *330*, 1648.

[4] K. Shibata, X. Z. Yu, T. Hara, D. Morikawa, N. Kanazawa, *Nat. Nanotechnol.* **2013**, *8*, 723.

[5] X. Z. Yu, N. Kanazawa, Y. Onose, K. Kimoto, W. Z. Zhang, S. Ishiwata, Y. Matsui, Y. Tokura, *Nat. Mater.* **2011**, *10*, 106.

[6] W. Münzer, A. Neubauer, T. Adams, S. Mühlbauer, C. Franz, F. Jonietz, R. Georgii, P. Böni, B. Pedersen, M. Schmidt, A. Rosch, C. Pfleiderer, *Phys. Rev. B* **2010**, *81* 041203.

[7] I. Dzyaloshinsky, *J. Phys. Chem. Solids* **1958**, *4*, 241.

[8] T. Moriya, *Phys. Rev.* **1960**, *120* 91.

[9] T. Adams, A. Chacon, M. Wagner, A. Bauer, G. Brandl, B. Pedersen, H. Berger, P. Lemmens, C. Pfleiderer, *Phys. Rev. Lett.* **2012**, *108* 237204.

[10] S. Seki, X. Z. Yu, S. Ishiwata, Y. Tokura, *Science* **2012**, *336*, 198.

[11] F. Qian, L. J. Bannenberg, H. Wilhelm, G. Chaboussant, L. M. Debeer-Schmitt, M. P. Schmidt, A. Aqeel, T. T. M. Palstra, E. Brück, A. J. E. Lefering, C. Pappas, M. Mostovoy, A. O. Leonov, *Sci. Adv.* **2018**, *4*, 9.

[12] A. Chacon, L. Heinen, M. Halder, A. Bauer, W. Simeth, S. Mühlbauer, H. Berger, M. Garst, A. Rosch, C. Pfleiderer, *Nat. Phys.* **2018**, *14*, 936.

[13] A. Aqeel, J. Sahliger, T. Taniguchi, S. Mändl, D. Mettus, H. Berger, A. Bauer, M. Garst, C. Pfleiderer, C. H. Back, *Phys. Rev. Lett.* **2021**, *126* 017202.

[14] A. Maisuradze, Z. Guguchia, B. Graneli, H. M. Rønnow, H. Berger, H. Keller, *Phys. Rev. B* **2011**, *84* 064433.

[15] I. Levatić, V. Šurija, H. Berger, I. Živković, *Phys. Rev. B* **2014**, *90* 224412.

[16] M. Ozerov, J. Romhányi, M. Belesi, H. Berger, J.-P. Ansermet, J. van den Brink, J. Wosnitza, S. A. Zvyagin, I. Rousochatzakis, *Phys. Rev. Lett.* **2014**, *113* 157205.

[17] N. Ogawa, S. Seki, Y. Tokura, *Sci. Rep.* **2015**, *5*, 10882.

[18] D. Hirobe, Y. Shiomi, Y. Shimada, J.-I. Ohe, E. Saitoh, *J. Appl. Phys.* **2015**, *117*, 053904.

[19] V. Dyadkin, K. Prša, S. V. Grigoriev, J. S. White, P. Huang, H. M. Rønnow, A. Magrez, C. D. Dewhurst, D. Chernyshov, *Phys. Rev. B* **2014**, *89* 140409.

[20] G. Meunier, M. Bertaud, *J. Appl. Crystallogr.* **1976**, *9*, 364.

[21] H. Effenberger, F. Pertlik, *Monatsh. Chem.* **1986**, *117*, 887.

[22] J.-W. G. Bos, C. V. Colin, T. T. M. Palstra, *Phys. Rev. B* **2008**, *78* 094416.

[23] M. Belesi, I. Rousochatzakis, H. C. Wu, H. Berger, I. V. Shvets, F. Mila, J. P. Ansermet, *Phys. Rev. B* **2010**, *82* 094422.

[24] J. Legma, G. Vacquier, A. Casalot, *J. Cryst. Growth* **1993**, *130*, 253.

[25] T. Schwarze, J. Waizner, M. Garst, A. Bauer, I. Stasinopoulos, H. Berger, C. Pfleiderer, D. Grundler, *Nat. Mater.* **2015**, *14*, 478.

[26] A. Aqeel, I. J. Vera-Marun, B. J. van Wees, T. T. M. Palstra, *J. Appl. Phys.* **2014**, *116*, 153705.

[27] A. Klein, Y. Tomm, R. Schlaf, C. Pettenkofer, W. Jaegermann, M. Lux-Steiner, E. Bucher, *Sol. Energy Mater. Sol. Cells* **1998**, *51*, 181.

[28] G. Prasad, O. N. Srivastava, *J. Phys. D: Appl. Phys.* **1988**, *21*, 1028.

[29] V. Chizhikov, V. Dmitrienko, *J. Magn. Magn. Mater.* **2015**, *382*, 142.

[30] V. Dmitriev, D. Chernyshov, S. Grigoriev, V. Dyadkin, *J. Phys.: Condens. Matter* **2012**, *24*, 366005.

[31] I. Stasinopoulos, S. Weichselbaumer, A. Bauer, J. Waizner, H. Berger, S. Maendl, M. Garst, C. Pfleiderer, D. Grundler, *Appl. Phys. Lett.* **2017**, *111*, 032408.